NACA RM A57I26

RESEARCH MEMORANDUM

EXPERIMENTAL INVESTIGATION OF THE SIMULATION OF ATMOSPHERIC ENTRY OF BALLISTIC MISSILES

By Stanford E. Neice, James A. Carson, and Bernard E. Cunningham

Ames Aeronautical Laboratory
Moffett Field, Calif.

NATIONAL ADVISORY COMMITTEE FOR AERONAUTICS

WASHINGTON

December 12, 1957

[redacted]

NATIONAL ADVISORY COMMITTEE FOR AERONAUTICS

RESEARCH MEMORANDUM

EXPERIMENTAL INVESTIGATION OF THE SIMULATION OF ATMOSPHERIC ENTRY OF BALLISTIC MISSILES

By Stanford E. Neice, James A. Carson, and Bernard E. Cunningham

SUMMARY

A small-scale apparatus for simulating the motion and heating of ballistic missiles is described along with elements of design and operation. Experiments with the apparatus demonstrate that conditions for simulation are fulfilled according to the theoretical requirements.

A series of tests, with a copper-clad flat-faced cylinder, at an entrance velocity of 14,000 feet per second, are described. Test results were derived from detailed observation of the model in flight, observation of the recovered model, and spectroscopic analysis of illumination caused by model traverse. The model survived the aerodynamic heating effects which correspond to those for the atmospheric entry of an intermediate-range ballistic missile.

INTRODUCTION

A major problem confronting the designers of long-range ballistic missiles is the aerodynamic heating which occurs during entry into the atmosphere. The high heating rates may promote structural failure of the heat-absorbing medium. The failure of the heat shield can occur in many ways (ablation of the surface in large pieces, melting at unexpected hot spots, etc.). In addition, distortion of the surface contour may result in important deviations from the intended trajectory. The analytic solution of these problems requires an understanding of several complex phenomena about which little is known. Results of detailed aerodynamic tests in the laboratory are sometimes uncertain because it is difficult to duplicate all flight conditions. A solution to these problems can be obtained through full-scale flight tests, but such tests are very time consuming and expensive. The need for an experimental facility to determine effectiveness of proposed missile designs, using small-scale models,

[redacted]

[redacted]

is therefore indicated. Thus we are led to the concept of an atmospheric-entry simulator in an effort to bridge the gap between detailed aerodynamic research and flight tests.

Such an atmospheric-entry simulator has been proposed in reference 1. The apparatus employs a free-flight model, geometrically similar to and made of the same material as the particular missile under consideration. The model is launched from a hypervelocity gun upstream through a specially designed supersonic nozzle. The gun provides the model with the velocity at which the missile enters the atmosphere and the nozzle generates a scaled approximation to this atmosphere. If the model and supersonic nozzle are properly scaled, the speed and Reynolds number of the full-scale missile will be duplicated by the model throughout its traverse through the nozzle. It is theoretically demonstrated in reference 1, with the aid of the analysis contained in reference 2, that the aerodynamic heating and thermal stresses experienced by a ballistic missile during atmospheric entry tend to be duplicated in the proposed apparatus.

A small-scale atmospheric-entry simulator has been put into operation at the Ames Aeronautical Laboratory. This report described in detail the operation of the apparatus and presents an analysis of data obtained from one configuration tested. Spectrographic records of the model during entry into the simulated atmosphere are presented.

NOTATION

a	speed of sound
A	reference area for drag evaluation, cross-sectional area
A'	launch tube cross-sectional area
C_D	drag coefficient, $\frac{\text{drag}}{\frac{1}{2}\rho V^2 A}$
$C_{f'}$	equivalent skin-friction coefficient
D	diameter
H_{av}	average heat transfer per unit area
H_s	heat transfer per unit area to stagnation point
L	over-all length
m	mass

M	Mach number
p	pressure
Q	total heat transfer
r	radius
R	total range of missile
S	surface area
t	time
T	absolute temperature
u	projectile velocity
$\overline{u}$	dimensionless projectile velocity (eq. (B6))
V	model or missile velocity
W	weight
x	distance in test chamber from reservoir
y	altitude
z	distance through launch tube
$\overline{z}$	dimensionless distance (eq. (B9))
β	constant in altitude-density relation (eq. (A1))
γ	ratio of specific heats of a gas
θ	angle of missile flight path to horizontal
ρ	density
σ	modified speed of sound (eq. (B7))
Σ_a	primary shock wave (fig. 12)
Σ_b	reflected shock wave (fig. 12)

Standard chemical symbols are used in designating elements and compounds.

Subscripts

o	condition at sea level
1,...,5	condition at various states in shock-tube process (fig. 12)
e	condition at entrance to earth's atmosphere
H	evaluation of density ratio, $\frac{\rho}{\rho_r}$, determined by pitot-tube measurements
mi	missile
mo	model
p	evaluation of density ratio, $\frac{\rho}{\rho_r}$, determined by static tube measurements
r	reservoir condition

APPARATUS AND TESTS

Small-Scale Atmospheric-Entry Simulator

Figure 1 is a schematic diagram of the apparatus, indicating the component parts. The apparatus consists of four main parts: pressure tank, test section, vacuum tank, and model launcher. The pressure tank is initially separated from the test section by a diaphragm which can be ruptured to permit the high-pressure air in the reservoir to flow through the test section into the vacuum tank. The model launcher serves to put aerodynamic models into flight, at the speed desired, upstream along the axis of the test section. The conditions of the flight are adjusted to simulate atmospheric entry. The theoretical basis for the simulation is summarized in Appendix A. The test section, designed to duplicate an exponential density distribution (see eq. (A1)) corresponding to an altitude segment of the atmosphere of about 100,000 feet, has a square cross section which expands from a 3/4- by 3/4-inch square near the pressure reservoir to a 6- by 6-inch square at the exit section where the air-stream Mach number is about 5. The appropriate variation of cross-sectional area was determined from one-dimensional-flow

considerations. A square cross section was chosen so that plane windows could be mounted flush with the relatively flat side walls. Such windows would minimize optical distortion. A photograph showing the test chamber is presented as figure 2, and figure 3 is a section drawing of the chamber.

Calibration of the Test Section

The density variation through the test chamber was determined from measurements of side wall and center line static pressures and center line pitot pressures at three selected stations. Time variations of the required pressures were obtained from oscilloscope records of the output of strain-gage pressure cells mounted at the selected stations. The oscilloscope records showed pressure fluctuations to be sufficiently damped after 150 milliseconds to assume that steady flow had been established in the test section. Accordingly, the ratio of static density to reservoir density (150 milliseconds after rupture of the diaphragm) was calculated from the ratio of the three measured pressures to the reservoir pressure, assuming isentropic flow (ref. 3). The density distributions thus obtained are presented in figure 4 along with the original design distribution. Figure 4 has a logarithmic ordinate and linear abscissa; consequently, the exponential variation, $\rho/\rho_r = e^{-\beta x}$, appears as a straight line starting from $\rho/\rho_r = 1$ and having a slope equal to $-\beta$. As seen in this figure, the actual calibration values indicate a somewhat steeper slope than the design value ($\beta = 0.530$ ft^{-1}) and a small deviation from a straight line. The steeper slope is probably due to an overcorrection for boundary-layer effects and errors resulting from the assumptions of one-dimensional channel flow. These factors could also account for some of the deviation from the "straight line" exponential variation, although condensation of water vapor and liquefaction of the air in the last 10 to 12 inches of the test chamber may also produce noticeable effects. According to reference 4, the presence of such phenomena is evidenced by the higher densities obtained by the static-pressure measurements as compared with those obtained from the pitot tube.

Flow conditions in the region of the stagnation point were of greatest interest here since all models tested were very blunt in shape. Flow conditions at the front of a pitot tube resemble those on the face of a blunt body, in that re-evaporation of condensed air and water vapor will take place. For this reason density ratios obtained from pitot pressures were used in determining the exponent $\beta = 0.600$ ft^{-1} (see fig. 4). The greater decrease in actual density from the design value increases the range of simulated altitude from the design value of 100,000 feet to a value of 113,000 feet.

Timing and Shadowgraph Systems

The test chamber was equipped with instrumentation for obtaining velocity records and shadowgraph pictures of the models in flight (see figs. 1, 2, and 3). Seven photobeam stations, consisting of a light source and photoelectric tube on opposite sides of the channel, were placed along the length of the test section approximately 15 inches apart. As each photobeam is interrupted by the model, the time is recorded on an electronic counter and the subsequent spark-shadowgraph station is fired after a suitable time delay. Spark-shadowgraph stations were located about 7 inches from each photobeam station. Two shadowgraph stations and three photobeam stations are located on the portion of the test chamber which is inside the vacuum tank (see fig. 3).

Spectroscope

In order to examine luminescence of the model, which is the result of its high speed of flight, a spectroscope was installed at a window of the test-section chamber. This required the removal of the photobeam normally used at that station. The spectroscope station was 42 inches from the pressure reservoir. This is the position where the maximum convective heating rates would occur. Duration of illumination, from models passing this station, was determined from the time variation of the photocell output originally at this position, and was found to be about 10 microseconds. This was much too short to obtain a successful spectrograph from available commercial instruments. For this application a spectrograph was specially built which incorporated a large prism, each face being 4-5/8 inches long and 2 inches high, consisting of a glass shell filled with carbon disulphide. The combination of the large prism along with an 8-5/8-inch focal length lens gave an effective aperture ratio (f number) of about 3.2. The small aperture ratio along with a 0.020-inch slit was sufficient to obtain a spectrograph in spite of the short exposure duration, although resolution was sacrificed.

The range of wave lengths covered by the spectroscope is from about 4000 to 6500 Å. This spectroscope is limited in the violet region (<4000 Å) by the presence of glass in the optical system; and in the red region (>6500 Å) by the resolution of the instrument.

Helium Gun

The model launcher is a helium gun and is shown schematically in figure 5. The gun consists of two main parts: a .22-caliber launch barrel (in housing) and a 20-millimeter pump barrel which are connected

in such a way as to enable the placement of the model and a 0.030-inch-thick nylon shear disk at the barrel coupling. The shear disk provides a pressure seal between the two chambers. Details of the design, operation, and development of the helium gun are presented in Appendix B. At the muzzle end of the .22-caliber barrel, baffle plates are placed to reduce the action of expanding gases on the model immediately after launching. A vacuum manifold is incorporated ahead of the baffles to keep the .22-caliber barrel at as low a pressure as possible prior to firing. The blast cone functions to protect the gun from the shock wave, produced when the copper diaphragm between the high-pressure reservoir and the test section is ruptured, and to help keep the launch barrel at a low pressure by allowing the air stream entering the front to expand into a low pressure region inside the cone.

In the firing condition shown in figure 5, the .22-caliber barrel is at a near vacuum, the 20-millimeter barrel is sealed from the .22-caliber barrel by the shear disk, the powder charge is in place, and the breech block secures a seal at the breech end. The pump barrel can then be filled with helium under pressure.

Performance of the gun, under optimum firing conditions of helium pressure and powder charge, was evaluated by firing a series of nylon right circular cylinders of different lengths into a vacuum. The experimental results are presented in figure 6 which shows the observed effect of model weight on muzzle velocity. The maximum velocity of about 17,400 feet per second was obtained with models weighing 0.05 gram. Further reduction in weight resulted in failure of the model to withstand the launching pressures.

Models

Cylindrical models were chosen for initial tests in the simulator. Such models are easy to construct and approximate the blunt-nosed configurations currently planned for long-range ballistic missiles. Several launchings were made of models shaped as shown in figure 7. The models were constructed of nylon, with a 0.007-inch copper piece cemented to the forward circular face. The models weighed 0.140 gram. The 0.010-inch, 45° chamfer was incorporated to prevent contact between the edge of the copper face and the inside of the launch barrel.

Test Procedure

Testing was performed in the following manner. A copper diaphragm was placed between the high-pressure reservoir and the test section (see figs. 1 and 3) and the connection was secured. The model and shear disk

were placed in position at the large coupling in the helium gun. The vacuum tank, test section, and launch barrel were then evacuated to a pressure of about 1 millimeter of mercury. The helium gun was loaded and high-pressure reservoir was pressurized to the desired amount.

The diaphragm between the high-pressure reservoir and the test section was ruptured. This resulted in the formation of a strong shock wave which discharged through the test chamber into the vacuum tank and established supersonic flow in the test chamber. After a suitable time was allowed for this flow to stabilize, generally about 150 milliseconds, the helium gun was fired and the model was propelled upstream through the test section. As the model proceeded through the test section, a time-distance history was deduced from electronic counters which operate from the signals from the photobeam stations (fig. 1). From this history a velocity record was obtained. Each photobeam signal also triggered a spark-shadowgraph station through a time-delay circuit and a spark shadowgraph of the model was taken at a point down range of the photobeam. The model velocity was nearly zero about the time it reached the upstream end of the test section and hence the model could be recovered intact in the pressure reservoir. This is an extremely valuable feature since one of the most effective methods of extracting data from the simulator is by detailed examination of recovered models.

RESULTS AND DISCUSSION

Application to Full-Scale Missile

In these tests the missile model was launched at a velocity of 14,000 feet per second, relative to the air stream at the discharge end of the test section. Reservoir pressure at the time of launching was 217 pounds per square inch absolute. The dimensions of the full-scale missile were determined by the method of reference 1. The velocity variation with altitude was calculated for an entrance velocity of 14,000 feet per second and a drag coefficient, C_D, of 1.9. The theoretical velocities for the simulated missile, along with the experimental velocities obtained (from one time-distance history) for a model in the simulator, are plotted according to simulated altitude and presented in figure 8. The agreement between the theoretical and experimental values presented in figure 8 demonstrates that one of the requirements for simulation has been satisfied, namely, that the velocity at corresponding points in the trajectory be the same for model and missile. Actually the experimental velocities are somewhat lower than the theoretical values at the end of the trajectory. The terminal velocities are small in both cases. Since the total heat absorbed per unit mass is proportional to the difference in the square of entrance and terminal velocities, the error in simulation of the total heating per unit mass will be negligible. The slightly higher deceleration rate for the model will, however, produce slightly higher

heating rates and consequently higher thermal stresses in the model. Conclusions regarding thermal stress on the basis of model trajectory will, therefore, be somewhat conservative.

As indicated in figure 8, the simulated missile has a diameter of 2.67 feet and weighs 900 pounds. From reference 5, in which the optimum performance characteristics of ballistic missiles are evaluated, this simulated missile should have a range of about 1370 statute miles when fired at an exit angle of about 40° to the horizontal. The thickness of the copper face on the model was 0.007 inch and corresponds to a thickness of 1 inch for the full-scale vehicle.

The altitude range of the facility is from 58,000 feet to 171,000 feet. Although the lower 58,000 feet is eliminated, it is apparent from the velocity curve of figure 8 that any heating associated with the lower velocities in this region will be small compared to the total.

Shadowgraph Observations

Spark shadowgraphs obtained along the model's trajectory for one test flight are shown in figure 9. Figure 9(a) shows the model near the beginning of its entry. The simulated altitude is about 160,000 feet and its velocity is about 14,000 feet per second. Figure 9(b) shows the same model at a simulated altitude of 98,000 feet, traveling at a velocity of 10,300 feet per second. According to reference 2, this portion of the trajectory is where the maximum convective heat transfer occurs with the accompanying maximum thermal stresses. The model in this photograph appears to be distorted in the vicinity of the front face. However, this is apparently optical distortion, since physical distortion of this magnitude would undoubtedly lead to permanent distortion, and none was noted in the recovered models. Figure 9(c) shows the model at a simulated altitude of about 80,000 feet and a velocity of 7000 feet per second. The maximum deceleration occurred at a simulated altitude of about 85,000 feet (ref. 2). The model has passed this point and is still intact.

Observations of Recovered Models

Figure 10 is a photomicrograph of the copper face of a model before and after flight through the simulator. With regard to the model prior to firing, we can clearly see concentric machine marks as well as some small scratches and irregularities. The surface condition is considerably altered by traverse through the simulator. The most striking feature about the surface is, of course, the several small craters. There is some indication that these craters were formed by impact with impurities,

consisting mainly of minute particles of zinc-chromate paint, in the air stream which ranged in diameter from about 0.008 to 0.0001 inch.

Aside from the surface pitting, other interesting observations can be made. In particular we can see that only slight evidence exists of the concentric machine marks which were so prominent in the unfired model. Evidently a portion of the front face of the model has been melted. Another feature is the coloring of the copper face, particularly evident in the upper left sector of the model near the outer edge. This gradation of color is similar to that obtained on a rapidly cooled copper sheet where a portion of the sheet has been heated to a temperature on the order of 1000° to 1500° F, while adjacent areas were relatively cooler. The experimental work of reference 6, as well as the theoretical analysis of reference 7, indicates that the heat transfer is highest near the outer edge of a flat-faced model as used in these tests.

Spectroscopic Observations

A spectrograph of the emitted radiation caused by the traverse of the model near the point of maximum convective heating is shown in figure 11. The elements present, as identified by their characteristic wave lengths given in reference 8, are indicated.

One of the most prominent lines in figure 11 is that of helium at 5876 Å. The presence of this line, as well as the weaker line at 4471 Å, is due to the high-temperature helium, used in the model launcher, which moves into the test section after the model. The presence of a lithium line at 6103 Å is also quite evident. Lithium is detectable to about 5 parts in 10 million, but the source of such an impurity is not understood. A small amount of calcium impurity is evidenced by the weak, diffuse line at 4227 Å.

The bulk of detectable lines are copper, chromium, zinc, and titanium. Copper, of course, is expected since the formation of the craters in the face of the models (see fig. 10) as well as any ablation of the surface would undoubtedly result in a noticeable emission. The previous supposition that the craters are caused by impurities in the air stream is supported by the presence of chromium, zinc, and titanium - all major constituents of zinc-chromate paint used to coat the inside of the pressure reservoir.

The prominent lines of free oxygen and nitrogen are outside the range of the spectrograph (4000 to 6500 Å) and therefore could not be detected. The characteristic maximum wave length of the radical NO is 6600 Å. The radical may be present, as evidenced by the intense illumination above 6000 Å in figure 11. The lack of resolution in this region, however, precludes its detection. Water vapor should be detectable

through the presence of either the OH radical or hydrogen. Whereas the characteristic emission wave length for OH is about 2780 Å, and is outside the range of the instrument, the prominent hydrogen line at 4861 Å is not in evidence. Consequently, it is believed that any water vapor that is present is not dissociated.

CONCLUDING REMARKS

The results of this investigation have demonstrated that the exponential variation of density is correctly achieved in the simulator test section. Furthermore, the variation of the model's velocity during flight through the simulator agrees closely with that predicted for the flight of the missile through the atmosphere. From these observations, it is inferred that simulation of the atmospheric entry of ballistic missiles can be accomplished with an apparatus such as that used in this investigation.

The survival of the model in its traverse of the simulator suggests that an IRBM whose design is based on the particular model tested could also probably survive the convective heating associated with its entry into the earth's atmosphere.

The logical extension to this investigation is to duplicate these tests with a model of an intercontinental vehicle. This extension, however, will require a new model launcher to provide velocities on the order of 20,000 feet per second. It is also desirable to use larger models in order to facilitate the use of more complex shapes, characteristic of operational vehicles. This will also require a larger model launcher and, in addition, a larger test section to accommodate such models.

Ames Aeronautical Laboratory
National Advisory Committee for Aeronautics
Moffett Field, Calif., Sept. 26, 1957

APPENDIX A

BASIS OF SIMULATION AND PRACTICAL CONSIDERATIONS

The conditions of similitude, as defined in reference 1, are derived from the simplified equations of reference 2 for motion and convective heating of ballistic missiles. Thus for an isothermal atmosphere

$$\frac{\rho}{\rho_o} = e^{-\beta y} \tag{A1}$$

the following expressions were derived (see ref. 1):

Heat absorbed per unit mass at altitude y

$$\frac{Q}{m} = \frac{V_e^2}{4} \frac{C_f' S}{C_D A} \left[1 - \left(\frac{V}{V_e} \right)^2 \right] \tag{A2}$$

where

$$\left(\frac{V}{V_e} \right)^2 = e^{-\frac{C_D \rho_o A}{\beta m \sin \theta_e} e^{-\beta y}} \tag{A3}$$

Average rate of heat transfer per unit area

$$\frac{dH_{av}}{dt} = \frac{C_f' \rho_o V_e^3}{4} e^{-\beta y} e^{-\frac{3}{2} \frac{C_D \rho_o A}{\beta m \sin \theta_e} e^{-\beta y}} \tag{A4}$$

Rate of heat transfer to stagnation point

$$\frac{dH_s}{dt} = 6.8 \times 10^{-8} \sqrt{\frac{\rho_o}{r}} V_e^3 e^{-\frac{\beta y}{2}} e^{-\frac{3}{2} \frac{C_D \rho_o A}{\beta m \sin \theta_e} e^{-\beta y}} \tag{A5}$$

[redacted]

It was desired that the total convective heat per unit mass (eq. (A2)) and the thermal stress experienced during the atmospheric entry of a ballistic missile be duplicated in a small-scale model propelled through a small-scale atmosphere. In reference 1 it is shown that this can be done, for the most part, provided the following conditions are satisfied:

(1) The density ratio (eq. (A1)) should be the same at corresponding points in the full-scale and small-scale atmosphere.

(2) The model and missile must be geometrically similar and made of the same material.

(3) The entrance velocity, V_e, must be the same for model and missile.

(4) The velocities (eq. (A3)) as well as the Reynolds numbers must be the same for model and missile at corresponding points in the full-scale and small-scale atmosphere.

If these conditions are satisfied, the results of reference 2 demonstrate that, for a given ratio of missile to model diameter, the density level of the small-scale atmosphere is established as

$$(\rho_o)_{mo} = (\rho_o)_{mi} \left(\frac{D_{mi}}{D_{mo}}\right) \tag{A6}$$

and the length of the small-scale atmosphere shall be

$$L = \left(\frac{y_e - y}{\sin \theta_e}\right)_{mi} \left(\frac{D_{mo}}{D_{mi}}\right)^2 \tag{A7}$$

where $y_e - y$ is the portion of the real atmosphere which is being simulated.

Heating rates for the model will be greater than those for the full-scale missile by a factor equal to the ratio of missile to model size. Further investigation, however, revealed that exactly this ratio of heat rates was required in order that the thermal stresses be identical for model and missile (ref. 1).

It should be noted that heat transfer by radiation is not simulated. In addition, duplication of the stagnation enthalpy alone may not be sufficient to insure complete simulation, since dissociation is also influenced by pressure. The pressures must, of course, be different for the model and missile in order to duplicate Reynolds number. The possible

limitations arising from dissociation phenomenon is discussed in reference 1. At the velocities used in this investigation, however, the discrepancies in heat transfer resulting from differences of pressure between model and missile should be small.

The construction of a practical simulator required an appropriately designed test chamber and model launcher. With regard to the test chamber, it was found that any desired portion of the atmosphere could be duplicated by a specially designed supersonic nozzle. The results of reference 2 demonstrate that almost all of the aerodynamic heating associated with a relatively light ballistic missile occurs within a 100,000-foot altitude range. Corresponding density limits could be obtained between the reservoir and exit sections of a Mach number 5 supersonic nozzle. Appropriate intermediate densities could be obtained by proper geometry.

Unlike atmospheric air, the air in the test chamber is in motion, resulting in an effective increase in model velocity throughout its traverse and, particularly, an increase in entrance velocity, V_e, of about 2300 feet per second. The use of relative velocities in this manner is desirable since it results in a sizable increase in entrance velocity and is permissible so long as the velocity at corresponding points in the full-scale and small-scale atmosphere is preserved (see eq. (A3)).

The use of velocities relative to the air stream would not detract from the simulation of total convective heat input per unit mass, Q/m (eq. (A2)), for the higher relative entrance velocity, since Q/m depends on the difference between the squares of the entrance and terminal velocities of the model relative to the air stream. Heating rates and thermal stresses, however, will be slightly lowered, since the same quantity of heat will be transferred during a slightly longer time than that where the model is fired into still air at the same relative velocity.

[redacted]

APPENDIX B

THE HELIUM GUN

It has been demonstrated (refs. 9 through 12) that models can be launched at high muzzle velocities when propelled by a gas of low molecular weight (i.e., low acoustic impedance). In references 9 and 10 a method for launching small-caliber models is described. This method depends on adiabatic compression by a single-stroke piston to provide helium at high pressure and temperature as a propellant gas. A second method (see ref. 11) involves the combustion of a hydrogen-rich mixture of hydrogen and oxygen in helium to provide a heated light gas (mostly helium) at high pressures.

In view of certain limitations of the two methods, pointed out in reference 12, it was decided to develop a model launcher using nonisentropic shock compression to provide a small reservoir of high-temperature high-pressure helium as the propellant gas. It was proposed to use an exploding powder charge to produce a strong shock system in a pump tube containing helium. This method of producing a small reservoir of high-temperature high-pressure gas was successfully used in the hypersonic gun tunnel (ref. 13) and has the advantage that it requires no complex components. The launch tube would be placed in line with the pump tube to complete the apparatus.

Pumping Cycle Analysis

It was observed in reference 13 that the exploding gun powder provided strong shocks of a strength comparable to that produced by a chamber whose area was large compared to the area of the pump tube. On the basis of this observation, the so-called "infinite area inlet" condition was chosen for determining the strength of the shocks produced in the pump tube. An analysis of this special type of shock-tube process is contained in reference 14.

A diagram showing the pump-tube process is presented in figure 12. The basic assumption of an infinitely large powder gas chamber need be valid only for the time the model is in the launch tube. The properties of the helium in state 5 depend on the strength, p_2/p_1, of the primary shock Σ_a, and on the initial temperature and pressure of the helium in state 1. In turn, the strength of the primary shock depends on the initial properties of the powder gas as well as the geometry of the apparatus. For an assumed inlet area ratio, $A_4/A_1 \rightarrow \infty$ and $M_s > 1$, the pressure ratios and fluid velocities are given as follows (see ref. 14):

$$\frac{p_4}{p_2} = \frac{p_4}{p_3} = \left[\left(\frac{2}{\gamma_4+1} \right)^{1/2} \left(1 + \frac{\gamma_4-1}{2} M_3 \right) \right]^{\frac{2\gamma_4}{\gamma_4-1}} \tag{B1}$$

$$u_2 = u_3 = a_4 \left(\frac{\gamma_4+1}{2} \right)^{1/2} \left(\frac{M_3}{1 + \frac{\gamma_4-1}{2} M_3} \right) \tag{B2}$$

From equation (B2)

$$M_3 = \frac{1}{\frac{a_4}{u_3} \left(\frac{\gamma_4+1}{2} \right)^{1/2} - \left(\frac{\gamma_4-1}{2} \right)} \tag{B3}$$

Thus M_3 is determined, for given values of a_4 and γ_4, in terms of the fluid velocity in state 3 or state 2. However, for shock tubes in general,

$$\frac{u_2}{a_1} = \frac{u_3}{a_1} = \frac{(p_2/p_1) - 1}{\gamma_1 \left\{ \frac{\gamma_1-1}{2\gamma_1} \left[\left(\frac{\gamma_1+1}{\gamma_1-1} \right) \frac{p_2}{p_1} + 1 \right] \right\}^{1/2}} \tag{B4}$$

The properties of helium in state 5 depend on primary shock strength, p_2/p_1, as given in the following relations

$$\left.\begin{aligned}
\frac{T_5}{T_1} &= \frac{T_5}{T_2}\frac{T_2}{T_1} \\
\frac{T_5}{T_2} &= \frac{\frac{p_5}{p_2}\left(\frac{\gamma_1+1}{\gamma_1-1}+\frac{p_5}{p_2}\right)}{1+\frac{\gamma_1+1}{\gamma_1-1}\frac{p_5}{p_2}} \\
\frac{T_2}{T_1} &= \frac{\frac{p_2}{p_1}\left(\frac{\gamma_1+1}{\gamma_1-1}+\frac{p_2}{p_1}\right)}{1+\frac{\gamma_1+1}{\gamma_1-1}\frac{p_2}{p_1}} \\
\frac{p_5}{p_2} &= \frac{\frac{p_2}{p_1}\left(\frac{\gamma_1+1}{\gamma_1-1}+2\right)-1}{\frac{\gamma_1+1}{\gamma_1-1}+\frac{p_2}{p_1}}
\end{aligned}\right\} \quad (B5)$$

Thus for prescribed properties in states 1 and 4, equations (B1) through (B5) permit the determination of the relevant properties in states 2, 3, and 5 as a function only of the primary shock strength, p_2/p_1.

Launch Cycle Analysis

The analysis of the launching cycle (ref. 10) is made with the assumption that the pump tube contains an infinite volume of gas and has the same diameter as the launch tube. To account for the larger velocities resulting from the real case at hand, pump-tube diameter greater than launch-tube diameter, a "chamberage" correction (ref. 10) is applied to calculate muzzle velocities. Analysis of the launching cycle, to determine the muzzle velocity of the model, proceeds as follows:

The model velocity is expressed as

$$u = \bar{u}\sigma_5 \quad (B6)$$

where

$$\sigma_5 = \frac{2}{\gamma_5-1}a_5 \quad (B7)$$

The dimensionless projectile velocity, $\bar{u}$, is related to a dimensionless distance, $\bar{z}$, in the following manner

$$\bar{z} = \frac{\gamma_5-1}{2}\left\{\left[\frac{(2/\gamma_5+1)-(1-\bar{u})}{(1-\bar{u})^{\gamma_5+1/\gamma_5-1}}\right] + \frac{\gamma_5-1}{\gamma_5+1}\right\} \tag{B8}$$

where

$$\bar{z} = \frac{A' p_5}{m_{mo}\sigma_5^2} z \tag{B9}$$

and A' is the launch-tube area, m_{mo} is the model mass, and z is the launch-tube length. From equations (B6) through (B9) the model velocity can be determined as a function of distance traveled along the launch tube, for given model weight and conditions in state 5. The chamberage factor, varying from 1.0 to 1.1, is then applied to the calculated model velocities.

Performance Estimation

In order to estimate the performance of the helium gun, certain initial conditions had to be established. The properties of the powder gas after combustion were assumed to be those of a gas produced by a typical nitrocellulose powder. In reference 15 such a typical gas has a molecular weight of about 23.4, a ratio of specific heats, γ, of 1.25, and a speed of sound of about 3800 feet per second, corresponding to a mean temperature during burning of about 5400° R. A pressure of 75,000 psi was considered as the maximum safely attainable in practice and was the value consequently assigned to the pump-tube breech. Helium in the pump barrel was at room temperature, about 520° R.

On the basis of these initial conditions, the performance was calculated by assuming a shock strength, p_2/p_1, and determining the quantities p_4/p_1, p_5/p_1, and T_5/T_1 with the use of equations (B1) through (B7). The projectile velocity was then calculated with the use of equations (B6) through (B9). This procedure was followed for shock strengths, p_2/p_1, up to 26 for a projectile weighing 180 milligrams and a .22-caliber, 4.4-foot-long launch barrel, with and without a chamberage correction. The theoretical velocities reached a maximum at a shock strength $p_2/p_1 = 12$. The initial helium pressure, p_1, corresponding to this optimum condition was found to be 935 psia.

Performance Evaluation

The performance of the helium gun was evaluated by launching several models into an evacuated chamber. The evacuated chamber in this case was the test chamber of the small-scale atmospheric-entry simulator, which also served as a timing device through the use of the seven photobeam stations already positioned along its 8-1/2-foot length. Maximum pressures at the breech of the 20mm pump barrel and at the coupling between pump and launch barrels were measured with conventional crusher type pressure gages as discussed in reference 16.

The first phase of testing was to determine the charge (Hercules "Unique") of powder necessary to produce a breech pressure of 75,000 psi, with an initial helium pressure of 935 psia, and a 1-caliber nylon model weighing 0.160 gram. The results of this test series are shown in figures 13 and 14 where breech pressures and projectile velocities attained in vacuum firing are plotted as a function of powder charge. Throughout most of this test series, a 1/2-caliber nylon interface piston was used in the 20mm pump barrel to separate the powder gas from the helium. At a powder charge of 33 grams, unstable burning occurred which resulted in excessively high breech pressures (about 87,000 psi), as shown in figure 13, whereas a reduction of charge to 32.5 grams resulted in normal firing. On the basis of these tests it was decided that 32.5 grams of powder would produce a maximum safe velocity.

Two launchings were made at powder charges of 25 and 32.5 grams without the use of an interface piston in the 20mm pump barrel. The results of these firings (see fig. 14) indicated that higher velocities might be attained without the piston.

A second series of tests were performed to determine the effect of the interface piston as well as the effect produced by varying the initial helium pressure. Three firings with and without the interface piston were made with the maximum safe powder charge of 32.5 grams. Breech pressures were about 74,000 psi. The results of this series, presented in figure 15, determined the optimum helium pressure for each test condition and demonstrated that, near the optimum values, discarding the interface piston would result in a velocity increase of about 400 feet per second. It should be noted, however, that figure 15 indicates a very shallow optimum and that variations in helium pressure of 20 to 30 psi from the optimum value produce only a small velocity change.

A final series of tests were performed to determine the variation of projectile velocity with model weight. A series of .22-caliber nylon cylinders with weights from about 60 to 160 milligrams were launched with a 32.5-gram powder charge and initial helium pressure of about 935 psia. Breech pressures were about 74,000 psi while pressures at the coupling between the pump and launch barrels were about 60,000 psi. The results

presented previously in figure 6 show the observed effect of model weight on launching velocity and make a comparison with theoretical predictions including a 0-percent and 10-percent chamberage correction (ref. 10). Velocities of about 17,400 feet per second were obtained with models weighing 0.05 gram. Figure 6 also shows that the chamberage correction is applicable only to lightweight models, while velocities predicted for heavier models, 120 to 160 milligrams, agreed favorably with predictions neglecting chamberage effects.

The lengths of the pump and launch barrels should be properly adjusted in order to achieve the optimum performance commensurate with a given model weight and type of powder. The proper determination of these lengths requires a consideration of the processes and functions involved in the firing procedure. The main function of the pump barrel is to provide a volume of helium sufficient to propel the projectile through the launch tube. For a given bore dimension the pump barrel length will determine the available volume of helium. Lengthening the launch tube, for the purpose of increasing muzzle velocity (see eq. (B9)), will require a larger volume of helium and consequently a longer pump tube. Were it not for the rarefaction process which starts at the breech shortly after the initial pressure rise, it would appear that a very long launch barrel, and correspondingly large pump tube, would produce the highest velocities. The rarefaction wave, however, can overtake the model while it is still in the launch tube and reduce its acceleration. Because friction also acts to decelerate the model, barrel lengths must be limited to avoid this situation.

The present model launcher does not necessarily represent an optimum device. The launch and pump barrels were originally designed for other hypervelocity operations and were considered adequate for the present application. When the launcher was fired with the "Unique" type of powder, the results were sufficiently satisfactory and so the launcher was put directly to use with the small-scale atmospheric-entry simulator.

REFERENCES

1. Eggers, A. J., Jr.: A Method for Simulating the Atmospheric Entry of Long-Range Ballistic Missiles. NACA RM A55I15, 1955.

2. Allen, H. Julian, and Eggers, A. J., Jr.: A Study of the Motion and Aerodynamic Heating of Missiles Entering the Earth's Atmosphere at High Supersonic Speeds. NACA TN 4047, 1957. (Supersedes NACA RM A53D28)

3. Ames Research Staff: Equations, Tables, and Charts for Compressible Flow. NACA Rep. 1135, 1953.

4. Hansen, C. Frederick, and Nothwang, George J.: Condensation of Air in Supersonic Wind Tunnels and Its Effects on Flow About Models. NACA TN 2690, 1952.

5. Eggers, Alfred J., Jr., Allen, H. Julian, and Neice, Stanford E.: A Comparative Analysis of the Performance of Long-Range Hypervelocity Vehicles. NACA TN 4046, 1957. (Supersedes NACA RM A54L10)

6. Stoney, William E., Jr.: Local Heat Transfer to Blunt Noses at High Supersonic Speeds. NACA RM L57D25c, 1957.

7. Reller, John O., Jr.: Heat Transfer to Blunt Nose Shapes With Laminar Boundary Layer at High Supersonic Speeds. NACA RM A57F03a, 1957.

8. Anon.: Handbook of Chemistry and Physics. Thirty-sixth ed., Chem. Rubber Pub. Co., Cleveland, Ohio, 1954.

9. Workman, E. J.: Hydrogen Gun Development. NMSM/RDD/T-720, New Mexico School of Mines, Res. and Dev. Div., June 30, 1950.

10. Charters, A. C., Denardo, B. Pat, and Rossow, Vernon J.: Development of a Piston-Compressor Type Light-Gas Gun for the Launching of Free-Flight Models at High Velocity. NACA TN 4143, 1957. (Supersedes NACA RM A55G11)

11. Slawsky, Z. I.: Some Fundamental Theoretical and Experimental Studies in the Development of Hypervelocity Guns. Proc. Fin-Stabilized Ammunition Com., First Quart. Meeting, Picatinny Arsenal, May 2, 1956, pp. 84-106.

12. Seigel, A. E., and Slawsky, Z. I.: A Hypervelocity Gun Using a Shock-Compressed Steam-Heated Propellant. NAVORD Rep. 4345, Nav. Ord. Lab., Aeroballistic Res. Rep. 351, July 30, 1956.

13. Eggers, A. J., Jr., Hansen, C. Frederick, and Cunningham, Bernard E.: Theoretical and Experimental Investigation of the Effect of Yaw on Heat Transfer to Circular Cylinders in Hypersonic Flow. NACA RM A55E02, 1955.

14. Glass, I. I., Martin, W., and Patterson, G. N.: A Theoretical and Experimental Study of the Shock Tube. Inst. of Aerophysics Rep. No. 2, Univ. of Toronto, Nov. 1953.

15. Corner, J.: Theory of the Interior Ballistics of Guns. John Wiley & Sons, Inc., 1950.

16. Hayes, Thomas Jay: Elements of Ordnance. John Wiley & Sons, Inc., 1938.

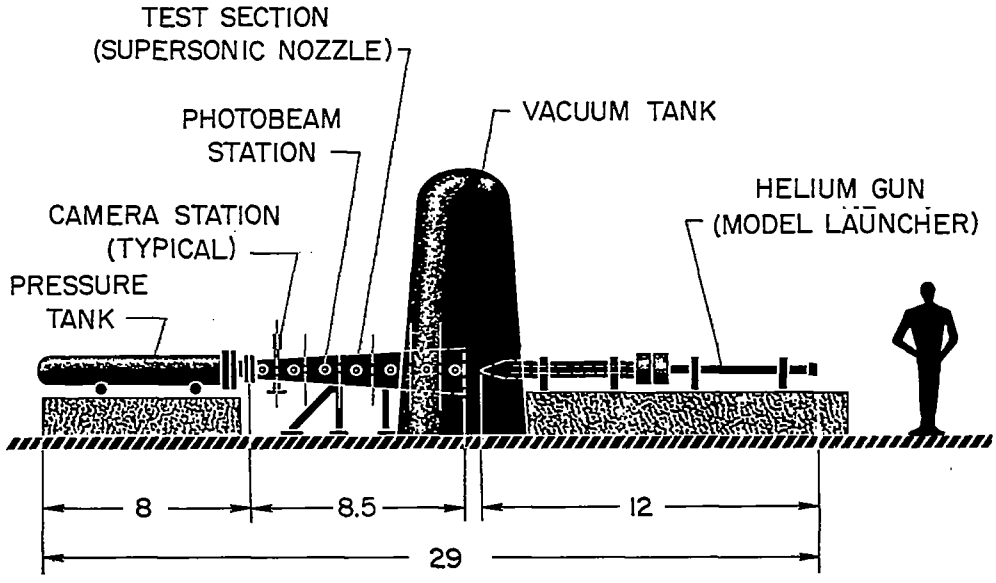

Figure 1.- Schematic diagram of small-scale atmospheric entry simulator; all dimensions in feet.

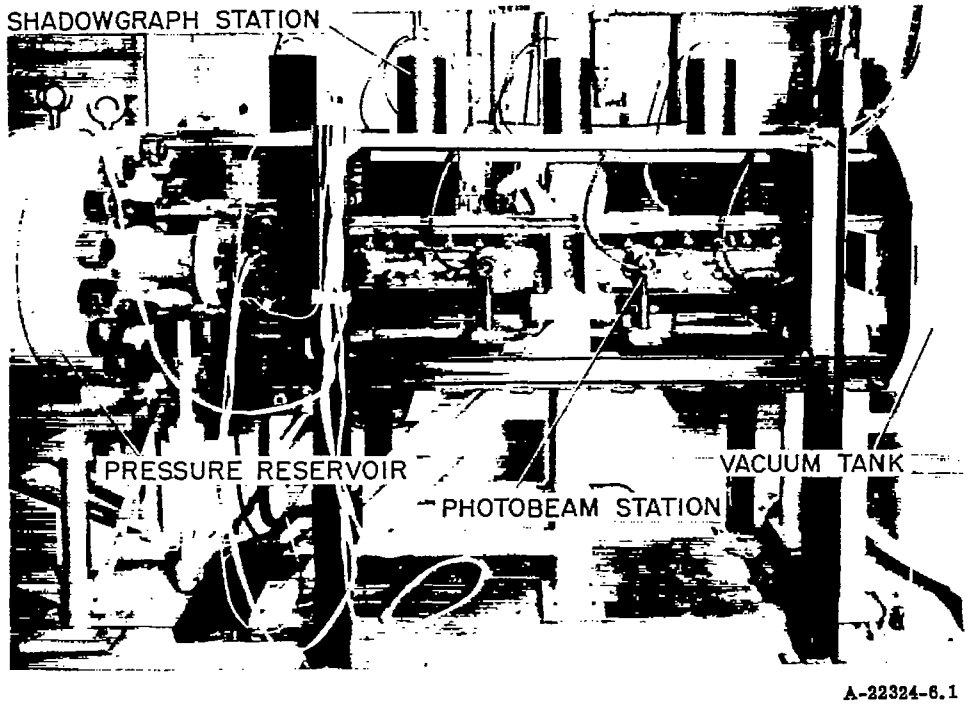

Figure 2.- Test chamber of small-scale atmospheric-entry simulator.

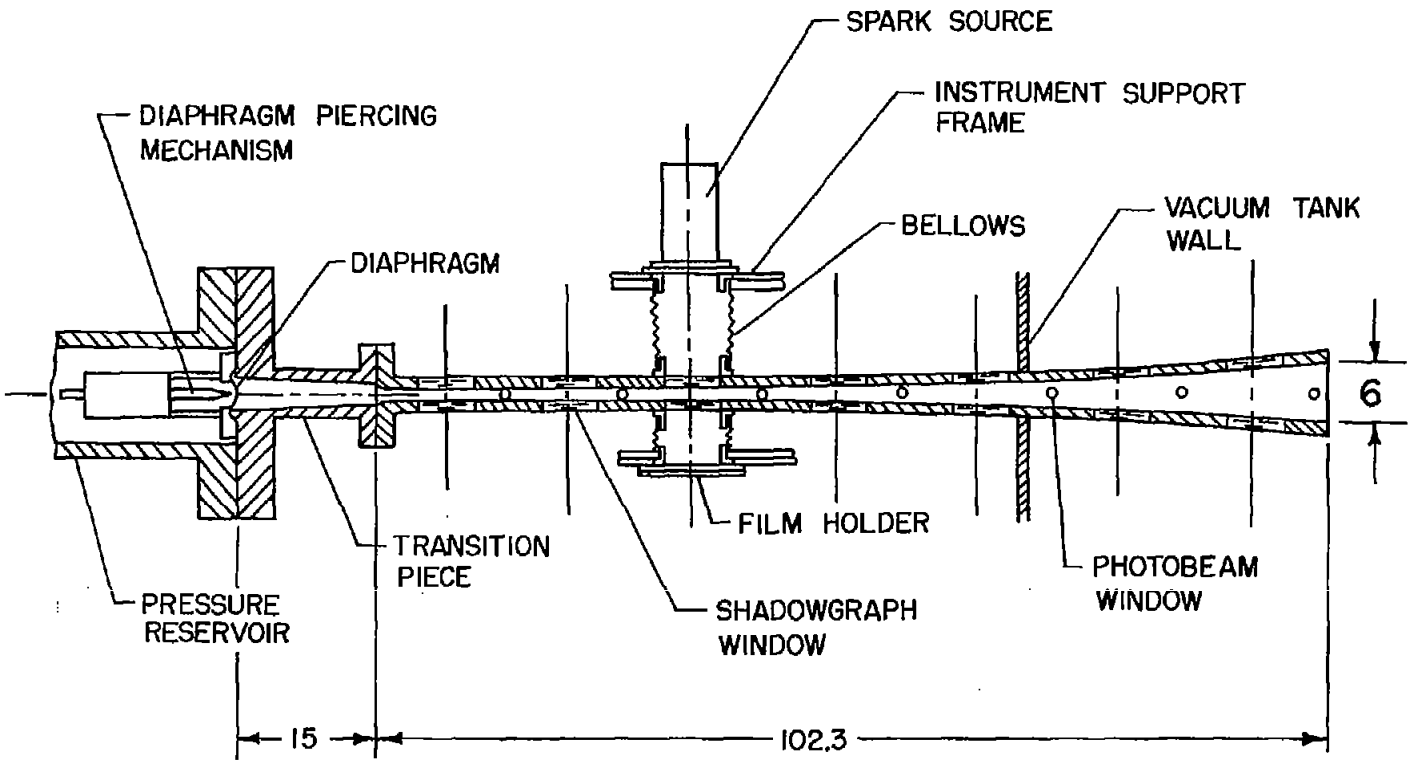

Figure 3.- Scale drawing of test section showing typical shadowgraph station and location of shadowgraph and photobeam stations; all dimensions in inches.

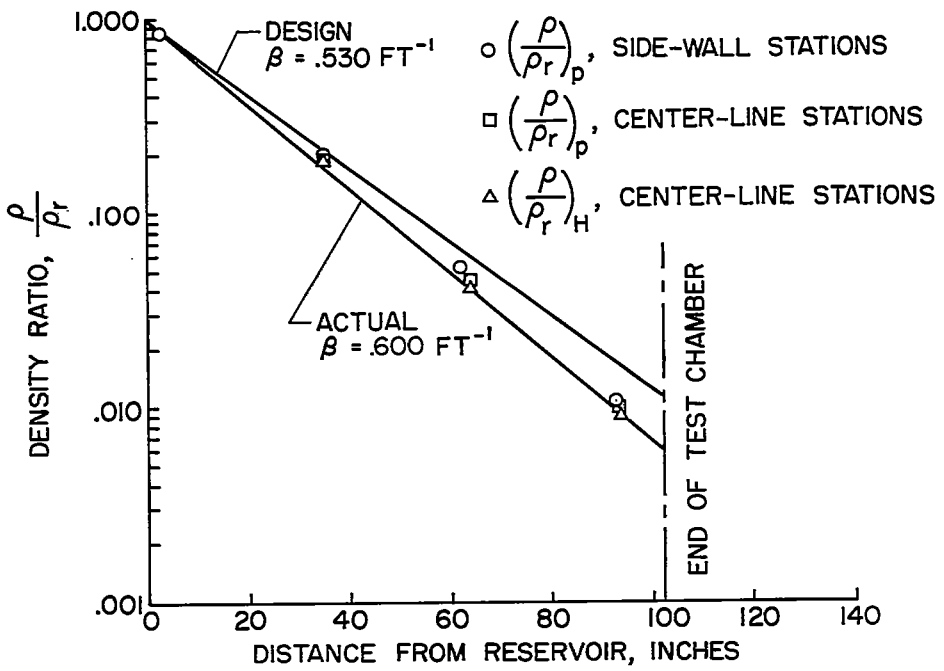

Figure 4.- Variation of density ratio with test section length.

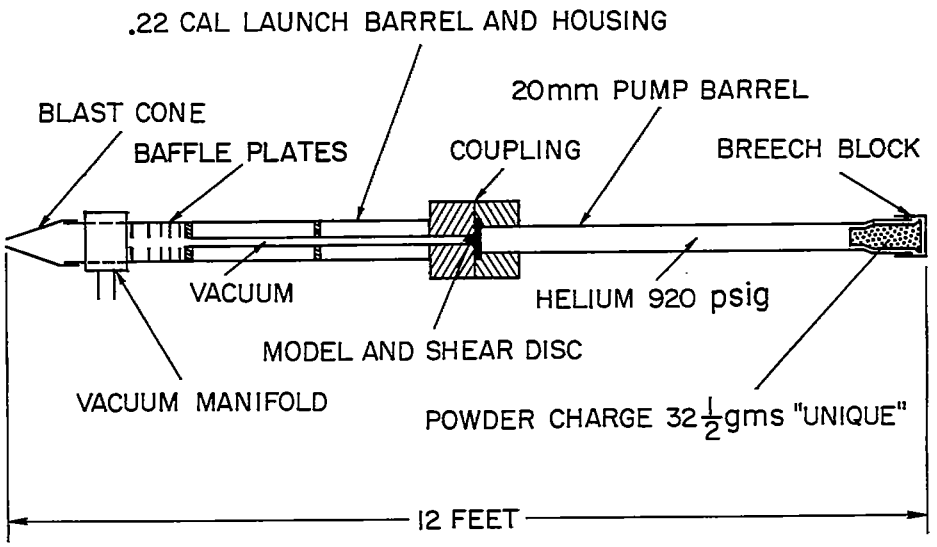

Figure 5.- Schematic diagram of helium gun.

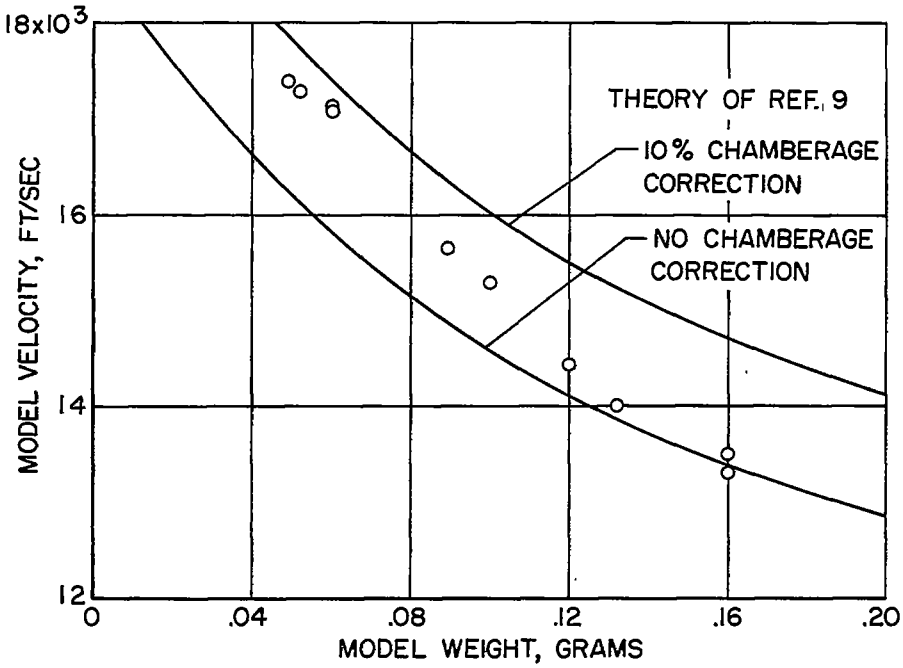

Figure 6.- Variation of model velocity with model weight; initial pump barrel helium pressure = 920 psig, powder charge = 32.5 grams.

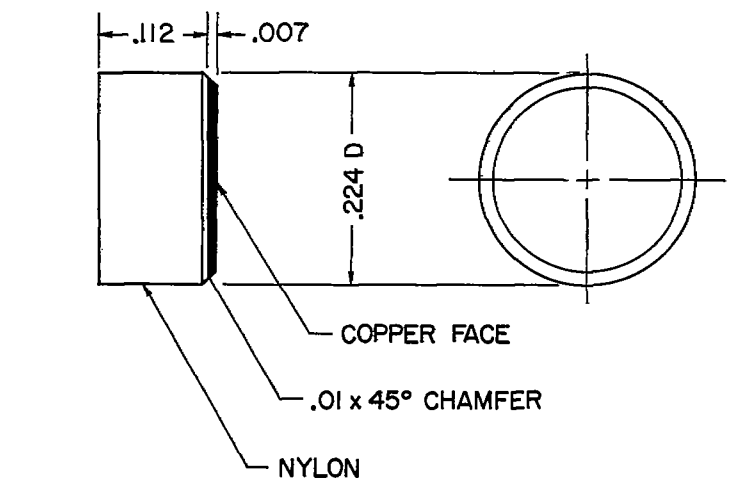

Figure 7.- Copper-faced models tested in small-scale atmospheric-entry simulator.

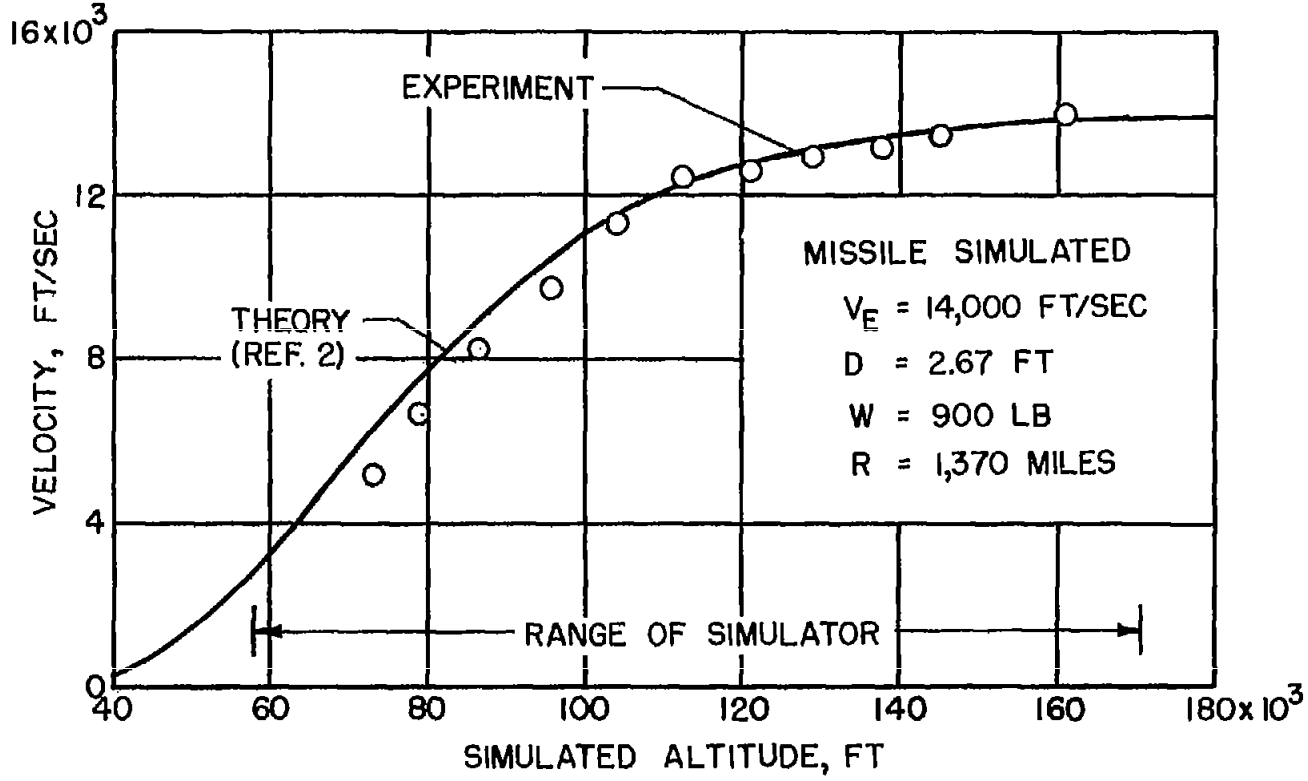

Figure 8.- Comparison of theoretical altitude variation of velocity for full-scale missile with experimental variation obtained with geometrically similar copper-faced model.

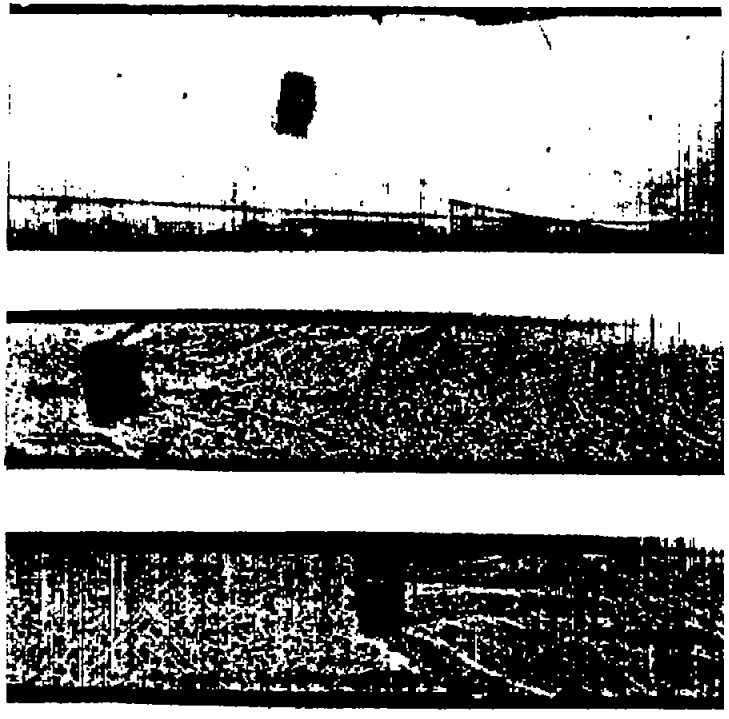

Figure 9.- Copper-faced model in flight through small-scale atmospheric-entry simulator.

Before test

After test

Figure 10.- Copper face of models before and after test in small-scale atmospheric-entry simulator; V_e = 14,000 feet per second, diameter = 0.224 inch.

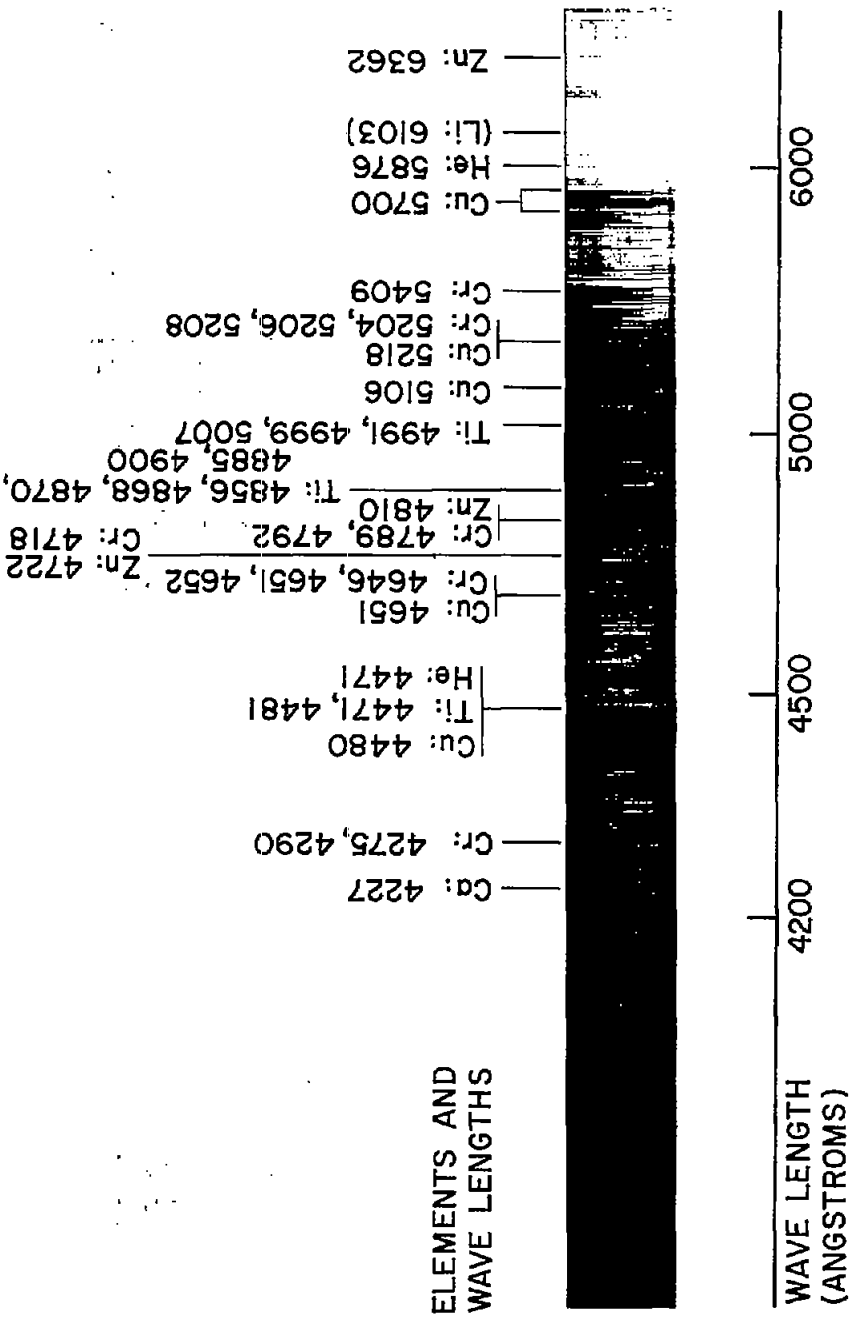

Figure 11.- Spectrum of illumination developed by copper-faced model at a simulated altitude of about 103,000 feet and a velocity of 11,400 feet per second.

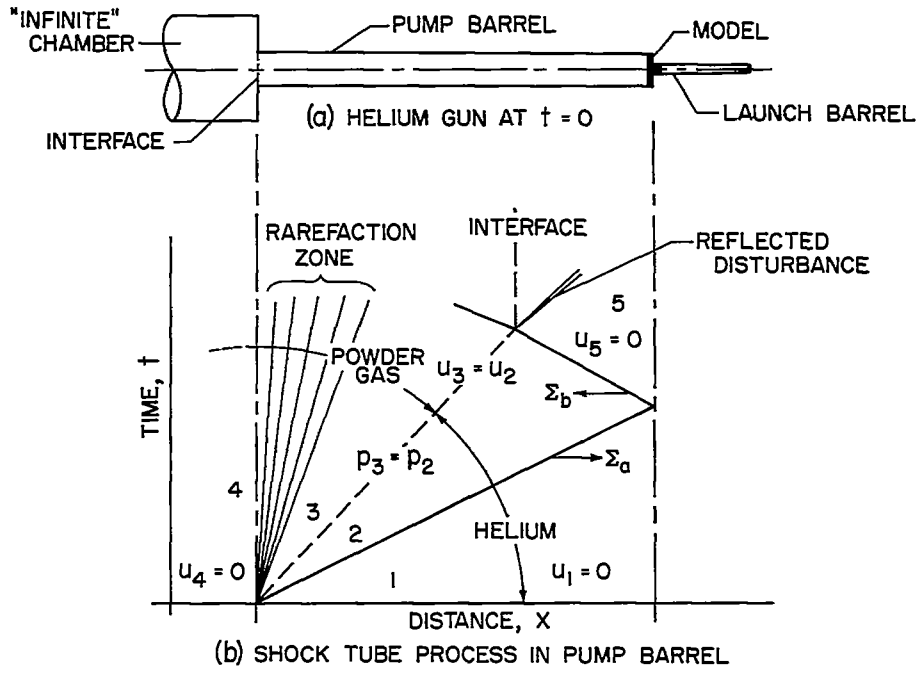

Figure 12.- Operation of helium gun pump barrel.

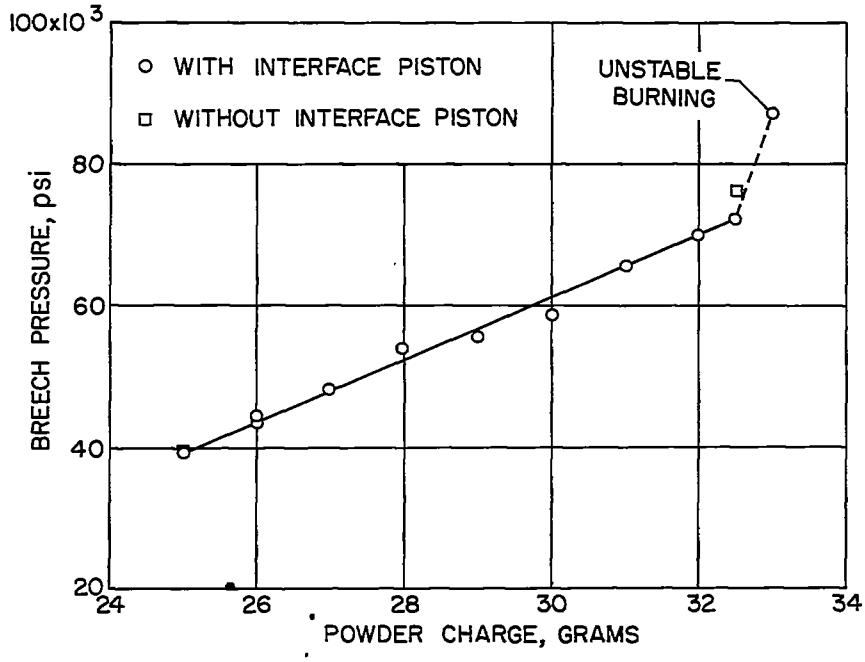

Figure 13.- Variation of breech pressure with powder charge for 0.16 gram model and pump tube helium pressure of 920 psig.

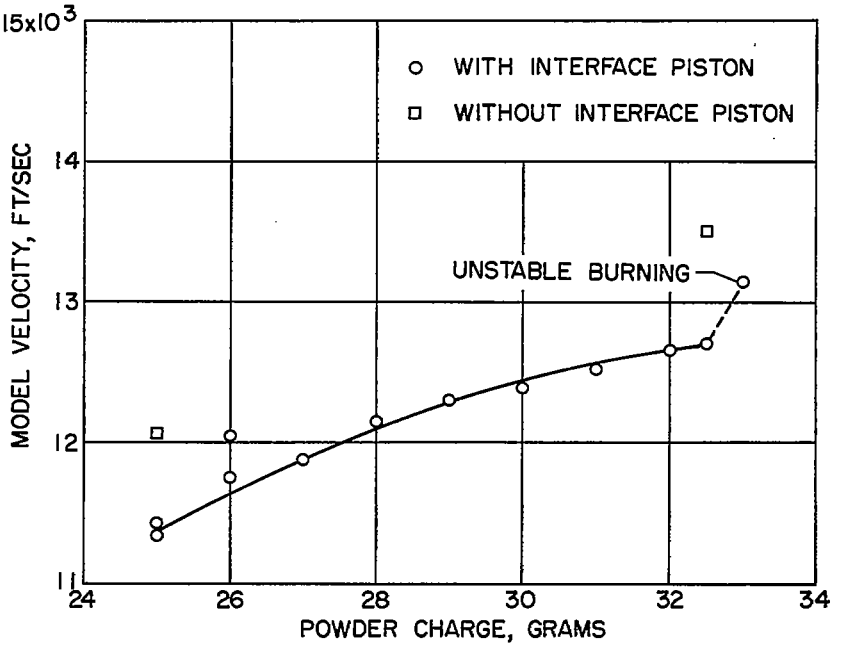

Figure 14.- Variation of model velocity with powder charge for model weight of 0.16 gram and pump tube helium pressure of 920 psig.

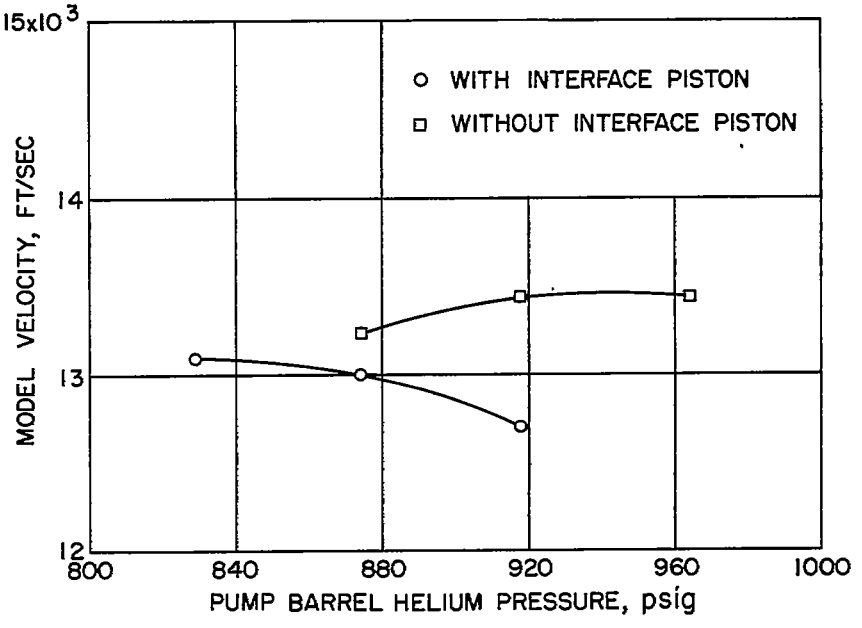

Figure 15.- Effect of interface piston on the variation of model velocity with pump barrel pressure for 0.16 gram model; 32.5 grams powder charge.

[redacted]

NACA - Langley Field, Va.